arXiv:1412.2823v1 [cond-mat.mes-hall] 9 Dec 2014

Decomposition into Propagating and Evanescent Modes of Graphene Ribbons

Hai-Yao Deng and Katsunori Wakabayashi*
International Center for Materials Nanoarchitechtonics (WPI-MANA),
National Institute for Materials Science (NIMS), Namiki 1-1, Tsukuba 305-0044, Japan
(Dated: December 10, 2014)

Bulk modes (BM) are basis solutions to the Schrödinger equation and they are useful in a number of physical problems. In the present work, we establish a complete set of BMs for graphene ribbons at arbitrary energy. We derive analytical expressions for these modes and systematically classify them into propagating or evanescent mode. We also demonstrate their uses in efficient electronic transport simulations of graphene-based electronic devices within both the mode-matching method and the Green's function framework. Explicit constructions of Green's functions for infinite and semi-infinite graphene ribbons are presented.

I. INTRODUCTION

Graphene, which is an atomically thick carbon sheet, and its nanostructures such as graphene nanoribbons continue to attract immense interest in the past decade due to their peculiar properties.[1–15] Numerous electronic devices[16] based on them, such as p-n junctions, field effect transistors and memory devices as well as electro-optical wave guides, have been studied extensively from both the theoretical[17–21] and experimental point of view.[22–24]

Theoretically, quantum transport simulations play an important part in understanding the behaviors of nano-devices.[25] Such simulations are generally based on Landauer-Büttiker picture[26–28] and can be implemented using either mode-matching[29–31] or Green's function approaches.[32–34] As shown by Khomyakov *et al.*,[35] these approaches are equivalent and their key quantities can be expressed in terms of the bulk modes (BMs), which are basis solutions (without satisfying all boundary conditions) to the Schrödinger equation and hence characteristic of the underlying Hamiltonian. However, a systematic exposure of such BMs for graphene structures has so far been wanting in the literature.

In the present paper, we systematically derive and classify the BMs (as either propagating or evanescent depending on their far-field behaviors) for graphene and graphene ribbons at arbitrary energy. Evanescent modes are known as the exponentially decaying or growing modes, which are induced at the edge surface or scattering center. We present those results for both armchair and zigzag ribbons. For graphene and armchair graphene ribbons (AGRs), the transverse (perpendicular to ribbon direction) and longitudinal (along ribbon direction) electronic motions are decoupled and hence analytical expressions for BMs can be obtained at arbitrary energy.[36,37] For zigzag graphene ribbons (ZGRs), these motions are not decoupled and analytical expressions are generally not available.[6,38] However, we derive a simple polynomial equation, which can be easily solved numerically, for locating the BMs of ZGRs. At low energies, simple analytical expressions are found to this equation.

A complete set of BMs is suitable for solving electron scattering problem of graphene nanostructures.[29,31,35,39] We demonstrate this by studying a graphene point contact in the mode-matching approach and by explicit construction of lattice Green's functions, which are essential in transport simulations of nano-devices,[34,40–42] for infinite and semi-infinite ribbons.

This paper is organized as follows. In the next section, we introduce the representation and derive the BMs for graphene. Then, in section III, we construct the BMs for ZGRs and thoroughly analyze their properties. Section IV is devoted to various applications as mentioned above. In Appendix A, we present results for AGRs. In Appendix B, we derive a useful formula for calculating group velocity of any mode.

II. BULK MODES OF GRAPHENE

Graphene has a honeycomb lattice structure of carbon atoms as shown in Fig. 1 (a). The x (y)-axis is taken along (perpendicular to) zigzag chains. For the purpose of this paper, we construct a supercell for the translational operation along x-axis, which is indicated as the rectangle region containing a single armchair chain in the figure. Since the honeycomb lattice is AB-bipartite, the atomic site on the n-th zigzag chain in the m-th supercell can be specified by three indices, (m, n, ν), where ν =A, B. For convenience, we define the sublattice index $\bar{\nu}$ to have the relations $\bar{\mathrm{A}}$ =B and $\bar{\mathrm{B}}$ =A. Throughout this paper, we choose the unit of length to be the lattice constant a, which is 0.142 nm.

We employ the nearest-neighbor tight-binding model to describe the electronic states of graphene. The Hamiltonian is written as

$$H = -\gamma_0 \sum_{\langle m,n,\nu,m',n'\rangle} |m,n,\nu\rangle\langle m',n',\bar{\nu}|, \tag{1}$$

where the summation is taken only for the pairs of nearest-neighbor carbon sites. γ_0 is the nearest-neighbor hopping energy which is approximately 2.7 eV. The Schrödinger equation for a given energy E is written as

$$H|F\rangle = E|F\rangle \tag{2}$$

with a generic solution $|F\rangle$, which can be decomposed as

$$|F\rangle = \sum_{m,n,\nu} F_\nu(m,n)|m,n,\nu\rangle. \tag{3}$$

The equation of motion for $F_\nu(m,n)$ is given by

$$\varepsilon F_\nu(m,n) = \sum_{m',n'} F_{\bar{\nu}}(m',n'), \tag{4}$$

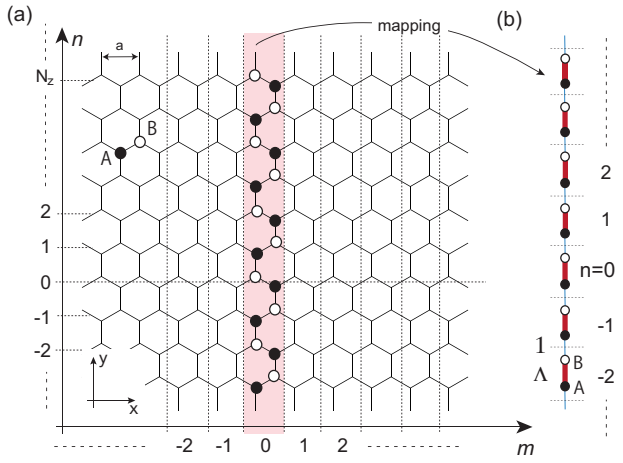

FIG. 1: (a) Schematic of graphene lattice. In the x-direction, the lattice is viewed as repetition of the supercell (numbered by m) indicated by the shaded rectangle. In the y-direction, the lattice is a collection of zigzag chains, which are labeled by n. A supercell extends from $n = -\infty$ to $n = \infty$. Each lattice site is specified as (m, n, ν), where $\nu = A, B$ refers to the sublattices. (b) By a transformation expressed in Eq.(6), the supercell is transformed into a diatomic chain. The effective hopping energies between adjacent sites are either Λ or 1, depending on whether the sites sit in the same zigzag chain or not.

where $\varepsilon = -E/\gamma_0$ is the dimensionless energy. Thus, $F_\nu(m, n)$ is given by the summation of its nearest-neighbors' $F_{\bar{\nu}}(m', n')$.

Since Eq. (4) is linear, any $F_\nu(m, n)$ can be resolved by a complete set of BMs. To obtain the BMs at arbitrary energy, we make use of the fact that the coefficients in Eq. (4) are independent of the supercell index m. Therefore, Blochesque ansatz[29,35] can be applied to Eq. (4), according to which $F_\nu(m, n)$ is related to $F_\nu(m-1, n)$ by the Bloch factor (a complex parameter) λ, i.e.,

$$F_\nu(m, n) = \lambda F_\nu(m-1, n) = \lambda^m F_\nu(0, n). \tag{5}$$

Note that within a supercell the relative position between the n-th A site and the n-th B site depends on the parity of n. To remove this dependence, we adopt the following transformation (with coordinates chosen in such a way that in the zigzag chain $n = 1$ the A site is to the left of the B site, see Fig. 1; otherwise, the following $\hat{M}$ matrix has be to replaced by its inverse),

$$\hat{f}(n) = \hat{M}^{-1}\hat{F}(0, n), \quad \hat{M} = \begin{pmatrix} \lambda^{\frac{(-1)^n}{4}} & 0 \\ 0 & \lambda^{-\frac{(-1)^n}{4}} \end{pmatrix} \tag{6}$$

where we have defined the spinors

$$\hat{F}(m, n) = \begin{pmatrix} F_A(m, n) \\ F_B(m, n) \end{pmatrix}, \quad \hat{f}(n) = \begin{pmatrix} f_A(n) \\ f_B(n) \end{pmatrix}. \tag{7}$$

After this transformation, the equation of motion for graphene is reduced to that for a diatomic linear chain as shown in Fig. 1(b). Substituting Eqs. (5) and (6) in Eq. (4), we arrive at

$$\begin{aligned} \varepsilon f_A(n) &= f_B(n-1) + \Lambda f_B(n), \\ \varepsilon f_B(n) &= f_A(n+1) + \Lambda f_A(n), \end{aligned} \tag{8}$$

where

$$\Lambda = \sqrt{\lambda} + \sqrt{1/\lambda}. \tag{9}$$

Now we can apply a similar Bloch ansatz regarding n, namely,

$$f_\nu(n) = \sigma^n f_\nu, \tag{10}$$

where $f_\nu := f_\nu(n = 0)$ and σ is another Bloch factor. Inserting Eq. (10) in (8), we get

$$\varepsilon \begin{pmatrix} f_A \\ f_B \end{pmatrix} = \begin{pmatrix} 0 & \Lambda + \frac{1}{\sigma} \\ \Lambda + \sigma & 0 \end{pmatrix} \begin{pmatrix} f_A \\ f_B \end{pmatrix}, \tag{11}$$

which is solved to yield

$$\begin{pmatrix} f_A \\ f_B \end{pmatrix} = \mathcal{N} \begin{pmatrix} s\sqrt{\Lambda + \sigma^{-1}} \\ \sqrt{\Lambda + \sigma} \end{pmatrix} =: \hat{f}_{\lambda\sigma s}, \tag{12}$$

and

$$\varepsilon^2 = (\Lambda + \sigma)(\Lambda + \frac{1}{\sigma}). \tag{13}$$

Here $\mathcal{N}$ is a normalization factor and $s = \pm$ indicates the sign of ε. Note that ε is symmetric with respect to λ and λ^{-1}, also with respect to σ and σ^{-1}. Thus, once we obtain the wavefunction for diatomic chain system for a given energy ε, the BMs for graphene can be obtained as a function of λ, σ and s through the following relation:

$$\hat{F}(m, n; \lambda, \sigma, s) = \lambda^m \sigma^n \hat{M} \hat{f}_{\lambda\sigma s}. \tag{14}$$

Although these modes are linearly independent of each other, they are not all orthogonal, because the square matrix in Eq. (11) is not hermitian in general. Note that Eq. (14) is obtained independent of boundary conditions and follows solely from the homogeneity (as embodied by the Bloch ansatz) and linearity of Eq. (4).

The boundary conditions for graphene are encoded in the translational symmetry along x- and y-directions, which require $|\lambda| = |\sigma| = 1$, i.e., $\lambda = e^{ik}$ and $\sigma = e^{ip}$, where k and p denote wave numbers in the range $(-\pi, \pi]$. The energy spectrum is then obtained as

$$\varepsilon = s\sqrt{1 + 2g_k \cos(p) + g_k^2}, \tag{15}$$

where $g_k := 2\cos(k/2)$. The celebrated Dirac points are located at $k = \pm\frac{2\pi}{3}$ and $p = \pi$.

III. MODE DECOMPOSITION OF ZIGZAG GRAPHENE RIBBONS

A. Derivation of basic equations

In this section we derive a complete set of BMs for ZGRs. These BMs can be classified as either propagating or evanescent, as described below. We assume that the ZGR has N_z

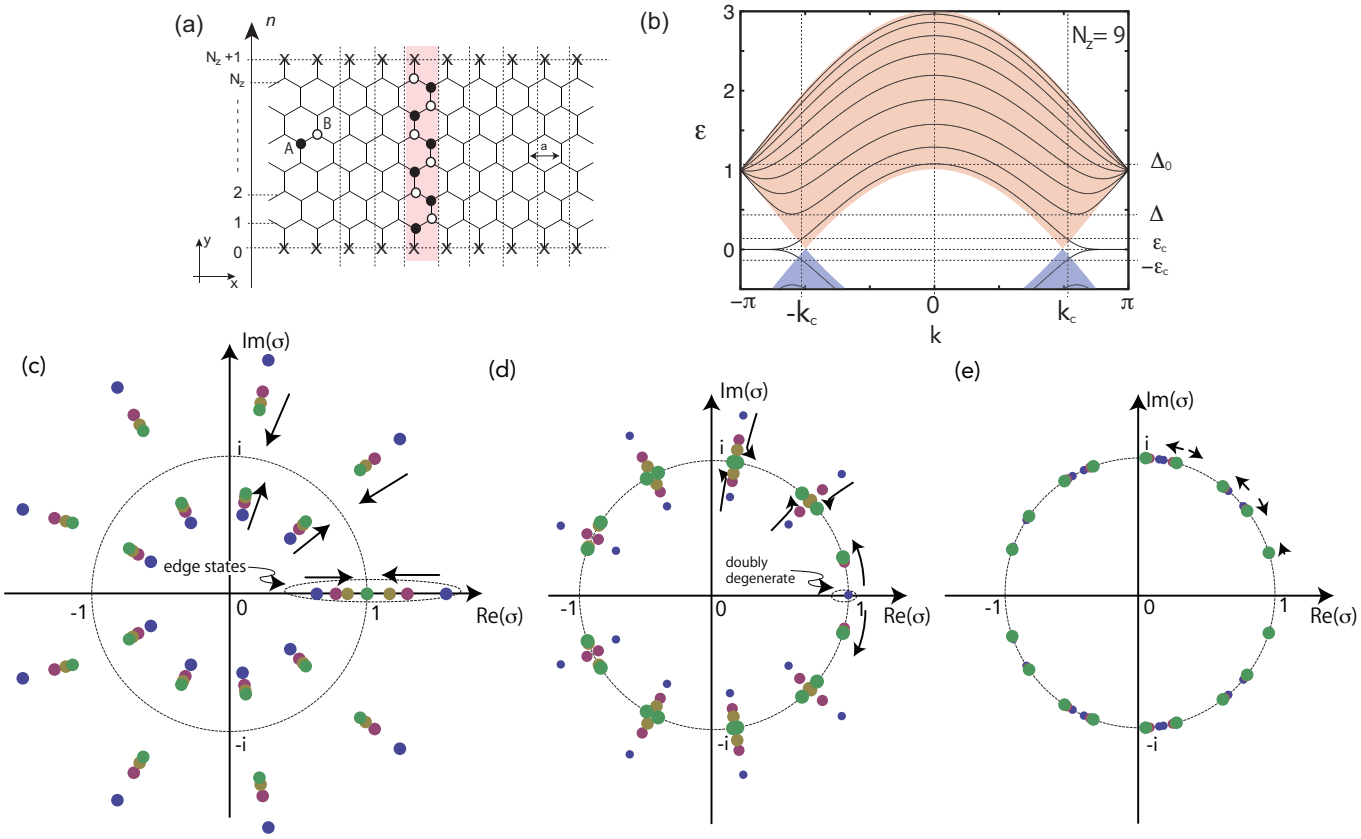

FIG. 2: (a) Schematic of ZGR lattice. The symbol "x" means that the wave function should be zero at this site. (b) Energy band structure of ZGR for $N_z = 9$. Shaded region represents the spectrum of graphene. (c) Distribution of roots of Eq. (24) in the complex σ-plane for the energy region $0 < |\varepsilon| \leq \varepsilon_c$. In this plot, the energies are taken as $\varepsilon = 0.01, 0.04, 0.07, 0.10$. The arrows indicate the direction of increasing energy. None of the roots (except when $|\varepsilon| = \varepsilon_c$; note $\varepsilon_c = 1/(N_z + 1) = 0.1$ for $N_z = 9$.) sit on the unit circle. (d) Same as (c) for the energy region of $\varepsilon_c \geq |\varepsilon| \leq 1$. In this plot, the energies are taken as $\varepsilon = 0.1, 0.4, 0.7, 1.0$. (e) Same as (c) for the energy region of $1 \leq |\varepsilon|$. In this plot, the energies are taken as $\varepsilon = 1.0, 1.5, 2.0, 2.5, 3.0$. Some of the circles are overlapping because of the tiny shift. Here all roots lie on the unit circle (dashed curve), i.e., $|\sigma| = 1$ and the resulting p are real.

zigzag chains in the region $0 < n < N_z + 1$. Let $\psi_\nu(m, n)$ denote the BMs together with its spinor representation:

$$\hat{\psi}(m, n) = \begin{pmatrix} \psi_{\rm A}(m, n) \\ \psi_{\rm B}(m, n) \end{pmatrix}. \tag{16}$$

The boundary conditions then require $\psi_B(m, 0) = 0$ and $\psi_A(m, N_z + 1) = 0$. Since the energy ε is invariant under $\sigma \to \frac{1}{\sigma}$, $\psi_\nu(m, n)$ can be simply derived from the linear combination of $\hat{F}(m, n; \lambda, \sigma, s)$ and $\hat{F}(m, n; \lambda, \sigma^{-1}, s)$, i.e.,

$$\hat{\psi}(m, n; \lambda, \sigma, s) = \lambda^m \hat{M}(\beta \sigma^n \hat{f}_{\lambda\sigma s} - \beta' \sigma^{-n} \hat{f}_{\lambda\sigma^{-1} s}). \tag{17}$$

Here β and β' are coefficients to be determined by the boundary conditions. Note that the $\hat{\psi}(m, n; \lambda, \sigma, s)$ and $\hat{\psi}(m, n; \lambda, \sigma^{-1}, s)$ represent the same BM.

By imposing the boundary conditions to Eq. (17), we obtain

$$\begin{pmatrix} z & -\frac{1}{z} \\ \Lambda + \sigma & -\left(\Lambda + \frac{1}{\sigma}\right) \end{pmatrix} \begin{pmatrix} \beta \\ \beta' \end{pmatrix} = 0, \tag{18}$$

where $z = \sigma^{N_z+1}$. Non-zero solutions exist if

$$z^2 = \frac{\Lambda + \sigma}{\Lambda + \frac{1}{\sigma}}. \tag{19}$$

Together with Eq. (13), this equation determines the allowed values of (λ, σ) at fixed energy ε.

By plugging it in Eq. (17), we find

$$\hat{\psi}(m, n; \lambda, \sigma, s) = \lambda^m \hat{\Phi}(n; \lambda, \sigma, s), \tag{20}$$

where

$$\hat{\Phi}(n; \lambda, \sigma, s) := \mathcal{N}' \hat{M} \begin{pmatrix} S_{N_z+1-n}(\sigma) \\ s(-1)^Q S_n(\sigma) \end{pmatrix}. \tag{21}$$

Here $\mathcal{N}'$ is a normalization factor and

$$S_n(\sigma) = \frac{1}{2i}\left[\sigma^n - \left(\frac{1}{\sigma}\right)^n\right]. \tag{22}$$

Q is an integer dictating the parity of the mode. Explicitly, we have[43]

$$(-1)^Q = z^{-1}\sqrt{\frac{\Lambda + \sigma}{\Lambda + \sigma^{-1}}}. \tag{23}$$

See that $\sigma = \pm 1$ lead to $S_n \equiv 0$, which must be excluded. These relations, $S_n(\sigma^{-1}) = -S_n(\sigma)$, $S_n(-\sigma) = (-)^n S_n(\sigma)$, generally hold.

B. Energy spectrum and number of modes

In this subsection we will show that the derived set of equations can correctly reproduce the energy band structure of ZGRs. To facilitate further analysis, we combine Eqs. (13) and (19) to get a polynomial equation of degree $4N_z$ for σ,

$$\left\{\mathcal{G}_{N_z}(\sigma^2) - \frac{\sigma^{N_z}}{\varepsilon}\right\} \cdot \left\{\mathcal{G}_{N_z}(\sigma^2) + \frac{\sigma^{N_z}}{\varepsilon}\right\} = 0. \tag{24}$$

Here $\mathcal{G}_{N_z}(x) = 1 + x + x^2 + ... + x^{N_z}$ and we have already excluded one pair of the unwanted roots $\sigma^2 = 1$. In addition, the Λ is derived from σ using the following relation

$$\Lambda = -\frac{S_{N_z}(\sigma)}{S_{N_z+1}(\sigma)}. \tag{25}$$

The energy spectrum for ZGR can be obtained if we assume a conventional Bloch phase for $\lambda = \exp(ik)$, which immediately gives $\Lambda = 2\cos(k/2) =: g_k$. Then we arrive at

$$g_k = -\frac{S_{N_z}(\sigma)}{S_{N_z+1}(\sigma)}. \tag{26}$$

This relation was derived by one of us and is confirmed to reproduce the energy spectrum,[15] if we solve this equation under the condition that σ is either real or pure phase (see details in next subsection) for given k-values. The obtained energy band structure for $N_z = 9$ is shown in Fig. 2(b).

For convenience, let us define several energy scales.
(i) ε_{max}: The top of the highest conduction band. This also gives the bottom of the lowest valence band as $-\varepsilon_{max}$. For graphene, $\varepsilon_{max} = 3$. For finite N_z, we have[44] $\varepsilon_{max}^2 \approx 5 + 4\cos\left(\frac{3\pi}{3N_z+2}\right)$. For large N_z, we obtain $\varepsilon_{max} \approx 3[1 - (\frac{\pi}{3N_z})^2]$. As we can see from Fig. 2(b), there is no propagating mode, i.e. only evanescent modes, for $|\varepsilon| > \varepsilon_{max}$.
(ii) Δ: The energy that gives the range of the single-channel region, in which $|\varepsilon| \leq \Delta$.
(iii) Δ_0: The energy for the lowest conduction subband at $k = 0$. As can be seen from Fig. 2(b), there are only propagating modes (in total $2N_z$: N_z left-going and N_z right-going modes), i.e. no evanescent mode, in the energy range of $1 \leq |\varepsilon| < \Delta_0$.

C. Propagating and evanescent modes

For a given energy ε, once we obtain Λ using Eqs. (24) and (25), a pair of λs are obtained through the following relation:

$$\lambda_\pm = \frac{1}{2}\left\{\Lambda^2 - 2 \pm \sqrt{\Lambda^2(\Lambda^2 - 4)}\right\}. \tag{27}$$

If $0 < \Lambda^2 < 4$, λ takes complex values with $|\lambda| = 1$, which gives rise to propagating modes in the x-direction. Otherwise, $|\lambda| \neq 1$ and evanescent modes will appear instead. We shall use $\lambda(+)$ to denote right-going (propagating or decaying to the right) modes and $\lambda(-) = \lambda^{-1}(+)$ for left-going (propagating or decaying to the left) modes. Note that one value of σ is accompanied by a pair of BMs represented by $\lambda(\pm)$.

Equation (24) contains $4N_z$ roots of σ for a given energy ε. However, we show that these roots are four-fold redundant and there are actually only N_z physically distinguishable roots, which obtain $2N_z$ BMs (counting both left- and right-going modes, i.e., $\lambda(\pm)$) as expected on general grounds.[29,35] To this end, we observe that Eq. (24) obeys two symmetries: invariance under $\sigma \to \frac{1}{\sigma}$ and under $\sigma \to -\sigma$. Therefore, if σ is a root, then $\frac{1}{\sigma}$ and $-\sigma$ as well as $-\frac{1}{\sigma}$ must also be roots. Nevertheless, the BMs represented by these roots are physically identical (up to an irrelevant phase factor). In fact, we have $\hat{\psi}(m, n; \lambda_\pm, \sigma^{-1}, s) = -\hat{\psi}(m, n; \lambda_\pm, \sigma, s)$ and $\hat{\psi}(m, n; \lambda_\pm, -\sigma, s) = (-1)^{N_z+1}\hat{\psi}(m, n; \lambda_\pm, \sigma, s)$, as can be deduced from Eqs. (20)-(23). Thus, in spite of that Eq.(24) contains $4N_z$ roots, we have only N_z physically distinguishable roots (and hence $2N_z$ BMs) owing to these symmetries.

Below we analyze the roots of Eq. (24) in detail. The results are summarized in Table I. In general, σ is a complex value, i.e. $\sigma = e^{ip}$ with $p = \phi + i\eta$. According to above analysis, p and $-p$ as well as $p + \pi$ give the same mode. It then suffices to focus on the domain where $\eta > 0$ and $0 \leq \phi < \pi$, which contains a complete set of BMs for ZGRs. No multiple roots exist for Eq. (24) at any $\varepsilon \neq 0, 1$.[45]

When σ is real, i.e., $\phi = 0$ (or equivalently π), then $0 < \Lambda^2 < 1$, always leading to propagating modes. Actually, $p = i\eta$ corresponds to the edge states that exist at very low energies. Indeed, Eq. (24) gives

$$|\varepsilon| = \frac{e^{-\eta N_z}}{\mathcal{G}_{N_z}(e^{-2\eta})}, \tag{28}$$

The right-hand side of this equation is monotonically decreasing for $\eta \geq 0$, whose maximum appears at $\eta = 0$ and its value is $\frac{1}{N_z+1}$. This means that the edge states exist only if $|\varepsilon| \leq \varepsilon_c$, where

$$\varepsilon_c = \frac{1}{N_z + 1}. \tag{29}$$

The $|\Lambda|$ at ε_c can be obtained as $|\Lambda| = \frac{N_z}{N_z+1}$ by taking the limit of $\eta \to 0$ for Eq. (25). Using $\lambda = e^{ik}$ for propagating modes, the wavenumber corresponding to ε_c is then given by

$$2\cos\left(\frac{k_c}{2}\right) = \frac{N_z}{N_z + 1}, \tag{30}$$

according to Eq. (9). Thus, the condition of real value for σ determines the region for the edge states, i.e. $|k| \geq k_c$. This result is consistent with previously reported results.[15]

Next we consider when σ is a pure phase factor, i.e., $\eta = 0$. In this case, $\Lambda = -\frac{\sin(N_z\phi)}{\sin[(N_z+1)\phi]}$ [as inferred from Eqs. (22) and (25)] is real and both propagating and evanescent modes can appear depending on whether $|\Lambda| \leq 2$ or not. Actually, for ϕ close to the nodes of $\sin(N_z\phi)$, we find small $|\Lambda|$ and hence propagating modes; whereas for ϕ close to the nodes of $\sin[(N_z + 1)\phi]$, large $|\Lambda|$ results and we get evanescent modes. Within the range of $0 \leq \phi \leq \pi$, there are $N_z - 1$ solutions of $p = \phi$ satisfying Eq. (25) if $|\Lambda| < 1$, whereas N_z solutions if $|\Lambda| > 1$. The missing solution corresponds to the edge state discussed in previous paragraph.[15]

TABLE I: Classification of the roots of Eq. (24): $\sigma = e^{i\phi-\eta}$; 'phase': $|\sigma| = 1$; 'complex': $\mathrm{Im}(\sigma) \neq 0$; 'N.S.C.': no special constraints. ε_{max} is given in the main text. The first two columns express necessary and sufficient conditions, but the conditions in the last four columns may not be sufficient. We distinguish edge states from extended states, which both are propagating modes.

Type	$\lvert\lambda\rvert$	Λ^2	σ	ϕ	η	$\lvert\varepsilon\rvert$
Edge	$= 1$	$\in [0,1]$	real	$0, \pi$	N.S.C.	$< \frac{1}{N_z+1}$
Extended	$= 1$	$\in [0,4]$	phase	$\in (-\pi, \pi)$	0	$< \varepsilon_{max}$
Evanescent	$\neq 1$	$\notin [0,4]$	complex	$\neq 0, \pi$	N.S.C.	$\notin [1, \Delta_0]$

Another special limit is $\sigma \to 0$, in which $\Lambda \sim -\sigma \to 0$. This then corresponds to $k \to \pi$, the completely localized edge state, whose energy is exactly zero by Eq. (13). Now Eq. (24) becomes simply $\sigma^{2N_z} \to 0$, which has $2N_z$ identical roots $\sigma \to 0$. The only BM is the completely localized edge state, whose wave function vanishes everywhere except on the zigzag edges. Thus, the interior of the ZGR becomes completely irrelevant. We expect this picture to be reasonable even for small but non-vanishing ε. This observation has been recently utilized to account for a parity effect[46,47] occuring in ZGR p-n junctions.[48]

Since propagating modes carry the flux of current, they are directly involved in scattering and transport problems. In band structure, these modes are usually labeled by wave numbers k together with p and s, namely,

$$\hat{\psi}(m, n; k, p, s) := e^{ikm}\hat{\Phi}(n; k, p, s), \tag{31}$$

and the corresponding energy is denoted by $\varepsilon_{ps}(k)$. The group velocity is given as

$$v_{ps}(k) = \frac{\partial}{\partial k}\varepsilon_{ps}(k). \tag{32}$$

Right-going (left-going) propagating modes therefore have $v_{ps}(k) > 0$ ($v_{ps}(k) < 0$). In Appendix B, we give a different expression for $v_{ps}(k)$, which is more useful in numerical computations.

D. Numerical analysis for σ

Figures 2 (c)-(e) show the distribution of roots of Eq. (24) in the complex σ-plane for some specific energies. Here we have numerically evaluated the roots of Eq. (24) using the Durant-Kerner-Aberth method.[49,50] The corresponding Λ^2 are calculated according to Eq. (25) to characterize the nature (propagating or evanescent) of the roots. The behaviors of the roots depend on the energy region.

1. For $0 < |\varepsilon| < \varepsilon_c$, none of the roots sit on the unit circle, see Fig. 2(c). The elevation of energy (along the arrows) shifts the roots toward the circle. In the plot, the energies are taken as $\varepsilon = 0.01, 0.04, 0.07, 0.10$ for the case of $N_z = 9$. Note that $\varepsilon = 0.10 \equiv \varepsilon_c$ for $N_z = 9$.

2. In the range $\varepsilon_c \leq |\varepsilon| < 1$, only those roots which represent propagating modes are located on the unit circle, see Fig. 2(d). In this plot, the energies are taken as $\varepsilon = 0.1, 0.4, 0.7, 1.0$. The arrow indicates the direction of increasing energy.

3. In the region of $1 \leq \varepsilon \leq \Delta_0$, all roots give rise to propagating modes and they lie on the unit circle. In the region of $|\varepsilon| \geq \Delta_0$, the roots still sit on the circle but their phases get shifted and some of them are converted into evanescent modes, see Fig. 2(e). In this plot, the energies are taken as $\varepsilon = 1.0, 1.5, 2.0, 2.5, 3.0$.

E. Analytical expressions for low-energy roots

The foregoing analysis renders analytical expressions for all the roots at $|\varepsilon| \ll 1$. To see this, we at first look at $|\varepsilon| \leq \varepsilon_c$. In such case, all roots have $|\sigma| \neq 1$ and they come in pairs, (σ, σ^{-1}). It suffices to find out those lying inside the unit circle, i.e., $|\sigma| \leq 1$. We denote such roots by x_r, where $r = 0, ..., N_z - 1$. Since $|x_r| < 1$, the expression $\mathcal{G}_{N_z}(x)$ in Eq. (24) may be approximated as $\mathcal{G}_{N_z}(x) \approx 1$ and hence, we obtain $x_r^{N_z} \approx |\varepsilon|$. From this, we find

$$x_r \approx |\varepsilon|^{\frac{1}{N_z}} e^{i\frac{\pi}{N_z}r}, \tag{33}$$

and then the complete set of roots is given as

$$\{x_0, x_0^{-1}, x_1, x_1^{-1}, ..., x_{N_z-1}, x_{N_z-1}^{-1}\}, \quad \text{for } |\varepsilon| < \varepsilon_c. \tag{34}$$

The pair that gives the edge state is (x_0, x_0^{-1}).

By increasing $|\varepsilon|$ above ε_c but below Δ, the edge state becomes an extended state, i.e., the pair (x_0, x_0^{-1}) is displaced onto the unit circle: $(x_0, x_0^{-1}) \to (e^{i\phi_0}, e^{-i\phi_0})$. Here ϕ_0 is the phase angle to be worked out later. On other hand, all other roots can still be well described by (x_r, x_r^{-1}), as is clear in Fig. 2(d). Thus, we find the complete set of roots to be

$$\{e^{i\phi_0}, e^{-i\phi_0}, x_1, x_1^{-1}, ..., x_{N_z-1}, x_{N_z-1}^{-1}\}, \text{for } |\varepsilon| \in [\varepsilon_c, \Delta). \tag{35}$$

To obtain ϕ_0, we substitute $\sigma = e^{i\phi_0}$ in Eq. (24) and find

$$\left|\frac{\sin\phi_0}{\sin(N_z+1)\phi_0}\right| = |\varepsilon|, \tag{36}$$

whose solution always lies in $(0, \frac{\pi}{N_z+1})$ for any $|\varepsilon| \in (\varepsilon_c, \Delta)$. For $|\varepsilon|$ slightly above ε_c, ϕ_0 is very small and we can then expand the left-hand side of this equation to get

$$\phi_0 \approx \frac{1}{N_z+1}\sqrt{\frac{6(|\varepsilon|/\varepsilon_c - 1)}{|\varepsilon|/\varepsilon_c - (N_z+1)^{-2}}}. \tag{37}$$

Although this expression has been derived by assuming that $|\varepsilon|$ be close to ε_c, it can actually describe the solution very

accurately in the whole regime (ε_c, Δ). In the limit $N_z \to \infty$, we find $\phi_0 \to \frac{\sqrt{6}}{N_z+1}$ for fixed $|\varepsilon|$, very close to the exact value of $\frac{\pi}{N_z+1}$.

By analogy with Eq. (35), one can write down sets of roots for even higher energy, but analytical expressions for the roots (more than one) on unit circles [i.e., of Eq. (36)] become impossible. The results contained in (34) and (35), supplemented by Eqs. (33) and (36), provide a complete foundation for studying e.g. quantum transport in a variety of ZGR junctions in the single-channel regime. There is no need to numerically search for the roots of Eq. (24) any more. The interrelation [Eq. (19)] between σ and λ becomes effectively dissolved.

IV. APPLICATIONS

This section is devoted to a few examples which illustrate common applications of the BMs we derived so far for graphene and graphene ribbons. A straightforward example is shown in the following subsection, where the electronic structure of bearded ZGRs is derived. Bearded ZGRs[51,52] are ZGRs with extra sites attached to one of its zigzag edges and they may be realized by chemical modifications. In another example presented in the second subsection we study quantum transport through a graphene aperture[53] using mode-matching method.[29] The BMs are then directly used in obtaining the transmission matrix. With the analytical prescriptions of the BMs, we can easily simulate ZGRs of width of hundreds of zigzag chains. Finally, in the third example considered in the third subsection, we relate the BMs to the core quantities of the widely employed nonequilibrium Green's function method[34] in transport simulations. We explicitly construct the Green's functions in terms of BMs.

A. Electronic structure of singly bearded ZGRs

Here we shall show that our approach correctly describes the energy spectrum and wave functions of singly bearded ZGRs. The lattice structure and energy band structure are shown in Figs. 3 (a) and (b), respectively. Since the system has the translational invariance along x-direction, we may assume that $\lambda = e^{ik}$. The boundary conditions requires for the wave functions can be written as $\psi_B(m, 0)$ and $\psi_B(m, N_z + 1)$.

For $\varepsilon \neq 0$, the σ can be shown to be a phase factor due to the boundary conditions. Thus, we put $\sigma = e^{ip}$. In analogy with Eq. (17), we can easily derive the wave functions to be

$$\hat{\psi}(m, n; k, p, s) \propto e^{ikm}\hat{M}\begin{pmatrix} s \cdot \sin(pn - \theta) \\ \sin(pn) \end{pmatrix}, \qquad (38)$$

where θ is the phase angle of $\gamma(k, p) =: g_k + e^{ip}$ and $p = \frac{\pi}{N_z+1} \cdot r$, with $r = 1, 2..., N_z$. The energy of this state is given by $\varepsilon_{kps} = s|\gamma(k, p)|$, by Eq. (13). Note that p does not depend on k, differing from the case with ZGR and doubly bearded ZGR.[51]

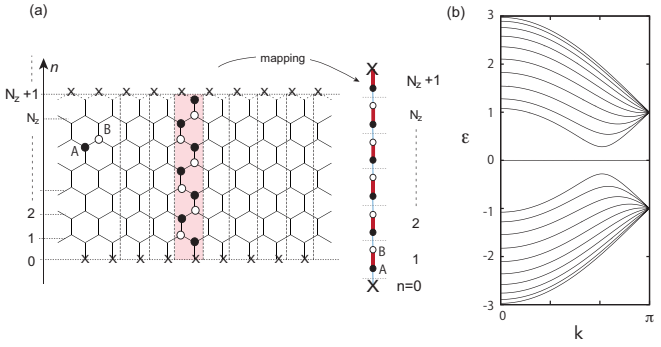

FIG. 3: (a) The lattice structure of singly bearded ZGR. (b) Energy band structure for $N_z = 10$. The central flat subband extends throughout the 1BZ.

For $\varepsilon = 0$, we have $\sigma = -g_k$ according to Eq. (13). The possibility that $\sigma = -g_k^{-1}$ is excluded by the boundary conditions. Denote the zero state by $\hat{\psi}_0(m, n)$ and we find

$$\hat{\psi}_0(m, n) \propto e^{ikm}\hat{M}\begin{pmatrix} (-2\cos\frac{k}{2})^n \\ 0 \end{pmatrix}. \qquad (39)$$

Here k can take any value between $-\pi$ and π, because $n = 1, 2, ..., N_z + 1$ is finite. Expectedly, these states are localized about the bearded edge if $|k| < \frac{2\pi}{3}$ but on the unbearded edge if $|k| > \frac{2\pi}{3}$.

Figure 3(b) shows the energy band structure for $N_z = 10$.[52] The central subband is completely flat, separated from the adjacent subbands by a gap of $\sin(\frac{\pi}{N_z+1})$ that is reached near the Dirac point.

B. Resonant transport through an aperture

In this subsection, we employ the BMs of ZGR to study electronic transport through a graphene aperture [see Fig. 4 (a)]. This type of aperture was studied by us[53] and it was analytically shown that peculiar low-energy resonant states could form due to the presence of edge states. In what follows, we revisit this phenomenon by a mode-matching approach. We perform numerical computations, on the basis of Eq. (24), to obtain the conductance through the aperture.

As clear from the energy band structure shown in Fig. 2(b), at a given ε, a propagating mode is specified by its k, which takes on discrete values $k_1, \bar{k}_1, ..., k_{N_p}, \bar{k}_{N_p}$. Here we reserve k_i for the i-th right-going mode while $\bar{k}_i = -k_i$ for the corresponding left-going mode. In general, we have $2N_p$ propagating modes, where factor 2 arises due to the fact that left-going and right-going modes come together. Accordingly, there are $N_e = N_z - N_p$ pairs of evanescent modes. In particular, for $|\varepsilon| < \Delta$, we have $N_p = 1$.

The size of the transmission matrix $\hat{t}(\varepsilon)$ is $N_p \times N_p$. Thus, let us denote the transmission coefficient from k_i to k_j mode as $t_{ji}(\varepsilon) := t_{k_j,k_i}(\varepsilon)$, where $i, j = 1, ..., N_p$. The conductance G

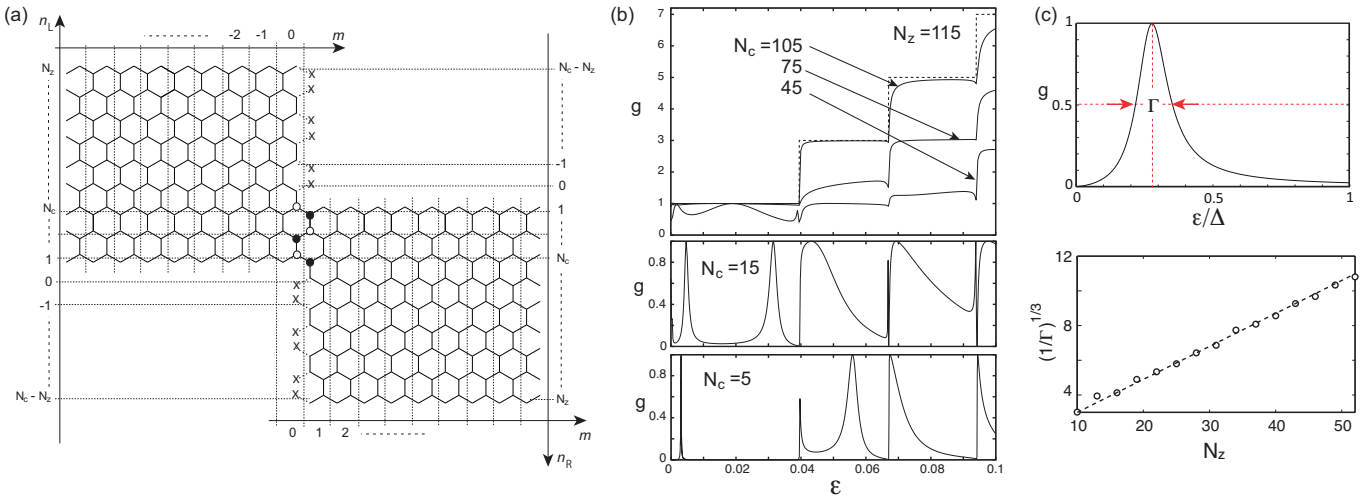

FIG. 4: (a) Structure of a graphene aperture connecting two graphene nanoribbons (width N_z), where the aperture consists of N_c connecting bonds. We use n_L and n_R to label the zigzag chains for the left and right nanoribbons, respectively. The local wave functions vanish on crossed sites while they match on the sites on connecting bonds marked by black and white circles. (b) The energy dependence of dimensionless conductance g for $N_z = 115$ and various N_c. (c) For $N_c \ll N_z$, the g shows a resonance of width Γ that scales as N_z^{-3}. The Δ is indicated in Fig. 2 (b).

is given by the Landauer-Büttiker formula:

$$G = \frac{2e^2}{h}\sum_{j=1}^{N_p}\sum_{i=1}^{N_p}|t_{ji}|^2 =: \frac{2e^2}{h}g, \tag{40}$$

where g is the dimensionless conductance.

Suppose an electron is injected upon the aperture from left at energy $\varepsilon > 0$ and with wave number k_i. It will be partially reflected into a mode of wave number $k_{i'}$ with amplitude $r_{i'i}$ and partially transmitted into a mode of wave number k_j with amplitude $\tilde{t}_{ji}$. Simultaneously, evanescent modes decaying away from the aperture will be excited. On the left-hand side to the aperture, the wave function can then be written as

$$\begin{aligned}\hat{\Psi}^L(m,n_L;k_i) &= e^{ik_i m}\hat{\Phi}(n_L;k_i) \\ &+ \sum_{i'=1}^{N_p} r_{i'i}e^{i\bar{k}_{i'}m}\hat{\Phi}(n_L;\bar{k}_{i'}) + \sum_{I=1}^{N_e} C_{Ii}^L\lambda_I^m\hat{\Phi}(n_L;I),\end{aligned} \tag{41}$$

where $\hat{\Phi}(n;k_i) := \hat{\Phi}(n;k_i,p_i,+)$ [see Eq. (31)], $\hat{\Phi}(n;I) := \hat{\Phi}(n;\lambda_I,\sigma_I,+)$ and C_{Ii}^L denotes the amplitudes for the I-th evanescent mode. Moreover, we require $v_{p_i+}(k_i) > 0$ and $v_{p_i+}(\bar{k}_i) < 0$ as well as $|\lambda_I| > 1$. Similarly, on the right-hand side, the wave function is given by

$$\hat{\Psi}^R(m,n_R;k_i) = \sum_{j=1}^{N_p}\tilde{t}_{ji}e^{ik_j m}\hat{\Phi}(n_R;k_j) + \sum_{J=1}^{N_e} C_{Ji}^R\lambda_J^m\hat{\Phi}(n_R;J). \tag{42}$$

Here we must have $|\lambda_J| < 1$. The $n_{L/R}$ in Eqs. (41) and (42) are defined in Fig. 4 (a). The $\tilde{t}_{ij}$ can be related to t_{ij} as follows,

$$t_{ji} = \sqrt{\frac{v_{p_j+}(k_j)}{v_{p_i+}(k_i)}}\cdot\tilde{t}_{ji}. \tag{43}$$

It should be noted that if the number of total connecting bonds (N_c) is even, the matrix $\hat{M}$ defined via Eq. (6) has to be replaced by its inverse in calculating $\hat{\Psi}^R(m,n_R;k_i)$.

The amplitudes $r_{i'i}$ and $\tilde{t}_{ji}$ are uniquely determined by the matching conditions appropriate for the aperture shown in Fig. 4 (a). Firstly, the $\hat{\Psi}^L(m,n_L;k_i)$ must vanish on all the crossed sites lying on $m = 1$, i.e.,

$$\begin{aligned}\Psi_A^L(1,N_c+2r+mod(N_c,2)+1;k_i) &= 0,\\ \Psi_B^L(1,N_c+2(r+1)-mod(N_c,2);k_i) &= 0.\end{aligned} \tag{44}$$

Besides, the $\hat{\Psi}^R(m,n_R;k_i)$ must vanish on all crossed sites lying on $m = 0$. Thus,

$$\begin{aligned}\Psi_A^R(0,N_c+2r+1;k_i) &= 0,\\ \Psi_B^R(0,N_c+2(r+1);k_i) &= 0.\end{aligned} \tag{45}$$

In the above, $r = 0,...,[N_z - N_c - mod(N_z - N_c,2)]/2 - 1$. Secondly, the $\hat{\Psi}^L(m,n_L;k_i)$ and $\hat{\Psi}^R(m,n_R;k_i)$ must be equal to each other on all the sites linked by the connecting bonds. Namely, we have

$$\begin{aligned}\Psi_A^L(0,2(w+1);k_i) &= \Psi_A^R(0,N_c+1-2(w+1);k_i),\\ \Psi_B^L(0,2w+1;k_i) &= \Psi_A^R(0,N_c-2w;k_i),\\ \Psi_A^L(1,2w+1;k_i) &= \Psi_A^R(1,N_c-2w;k_i),\\ \Psi_B^L(1,2(w+1);k_i) &= \Psi_B^R(1,N_c+1-2(w+1);k_i),\end{aligned} \tag{46}$$

where $w = 0,...,[N_c - mod(N_c,2)]/2 - 1$. Altogether, Eqs. (44) - (46) produce $2N_z$ independent conditions, which uniquely determine the $2N_z$ unknowns, $r_{i'i}$, $\tilde{t}_{ji}$, C_{Ii}^L and C_{Ji}^R.[48]

We have numerically calculated the Landauer conductance for a variety of structural parameters for the aperture. Since we know the analytic form of BMs, we can easily reach the relatively larger system over $N_z = 100$ with very little computation time. Fig. 4(b) shows the energy dependence of dimensionless conductance g for $N_z = 115$ with various N_c.

The decrease of N_c causes the reduction of conductance. In the region of $N_c \ll N_z$, the resonances appear in the low energy region. The origin of these resonances is attributed to the formation of quasi-bound states near the aperture due to the interference of edge states.[53] A typical behavior of lowest-energy resonance for $N_c \ll N_z$ is displayed in Fig. 4(c) Its width at the maximum is scaled with N_z following a power law, $\Gamma^{-1} \sim N_z^3$, in agreement with our analytical treatment.[53]

C. Green's functions of ZGR electrodes

In preceding subsection, the utility of BMs has been elucidated with the mode-matching method[29] and the conductance G of a graphene aperture was computed. In the literature, however, this conductance is more frequently evaluated by an apparently different method based on Green's functions.[34] The equivalence between the mode-matching and the Green's function methods have been demonstrated in Ref.[35]. In what follows we explain how to obtain the Green's functions in terms of the ZGR BMs.

We consider a general two-probe experimental setup as portrayed in Fig. 5, where a conducting channel or scattering region (represented by H_s) is connected to two electrodes via V_L and V_R, respectively. Both electrodes are represented by semi-infinite ZGRs. The left electrode extends from $m = 0$ to $m = -\infty$, whereas the right one from $m = 1$ to $m = \infty$. The V_L (V_R) couples only the supercell $m = 0$ ($m = 1$) to the channel. We shall write the Hamiltonian for the left electrode as $H_L = \sum_{m=0}^{-\infty}(H_m^m \oplus H_m^{m-1})$. Similarly, for the right electrode, $H_R = \sum_{m=1}^{\infty}(H_m^m \oplus H_{m+1}^m)$. Here H_m^m couples sites in the same supercell, while H_{m+1}^m couples sites in the m-th supercell to those in the $(m+1)$-th one (see Fig. 5). Since the block matrice $H_{m\pm1}^m$ are independent of m, we then put $V \equiv H_{m-1}^m$ and $V^\dagger \equiv H_{m+1}^m$. Further, we define a global block Green's function as $G_{m,m'}(\omega) = \langle m|(\omega - H_s - H_L - H_R)^{-1}|m'\rangle$, where ω is a complex parameter and H_s has included both V_L and V_R by definition. Now the conductance of the setup can be evaluated as[34,54]

$$g = \frac{2e^2}{h} Tr[\Gamma_R G^r \Gamma_L G^a], \tag{47}$$

where $G^r = G_{1,0}(\varepsilon + i0_+)$, $G^a = G_{0,1}(\varepsilon - i0_+)$. In addition, the broadening functions $\Gamma_{R/L}$ are given by

$$\Gamma_{R/L} = i(\Sigma_{R/L} - \Sigma_{R/L}^\dagger). \tag{48}$$

Below we prescribe the expressions for the self-energies $\Sigma_{R/L}$ in terms of the BMs.

At given energy ε, s is fixed and there are in total N_z values of σ, i.e., $\sigma_1, ..., \sigma_{N_z}$. For each σ_u, where $u = 1, ..., N_z$, there is a pair of λs [see discussions following Eq.(27)], $\lambda_u(+)$ and $\lambda_u(-) = \lambda^{-1}(+)$ standing for right-going and left-going modes, respectively. We define a number of column vectors by Eq. (21),

$$\Phi_u(\pm) := [\Phi_A(1;u), \Phi_B(1;u), ..., \Phi_A(N_z;u), \Phi_B(N_z;u)]^T, \tag{49}$$

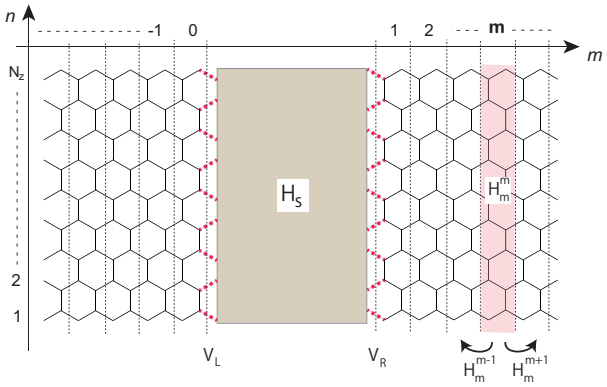

FIG. 5: A generic setup in two-probe transport measurements. The conducting channel, represented by the Hamiltonian H_s, is connected to the left electrode and the right electrode via couplings V_L and V_R, respectively. Both electrodes are represented by semi-infinite ideal ZGRs each consisting of N_z zigzag chains.

where $\Phi_\nu(n;u) := \Phi_\nu(n;\lambda_u(\pm),\sigma_u,s)$. Further, we introduce N_z pairs of dual vectors, $\tilde{\Phi}_u(\pm)$, uniquely defined by

$$\tilde{\Phi}_u^\dagger(\pm)\Phi_{u'}(\pm) = \delta_{uu'}, \quad \Phi_u^\dagger(\pm)\tilde{\Phi}_{u'}(\pm) = \delta_{uu'}. \tag{50}$$

Finally, we need the following $2N_z \times 2N_z$ matrix,

$$\mathcal{K}^r(\pm) = \sum_{u=1}^{N_z} \lambda_u^r(\pm)\Phi_u(\pm)\tilde{\Phi}_u^\dagger(\pm), \tag{51}$$

with r being an integer. For completeness, we sketch how to find the $\tilde{\Phi}_u(\pm)$ from $\Phi_u \equiv [\Phi_u(+), \Phi_u(-)]$. Let us define a $2N_z \times 2N_z$ matrix, $\mathcal{L}$, whose elements are given by $\mathcal{L}_j^i = \Phi_j^\dagger(i)$, and a number of $2N_z \times 1$ column vectors, $D_j(\pm)$, whose elements are given by $D_j(+, i \le N_z) = \delta_{ij}$, $D_j(+, i > N_z) = 0$, $D_j(-, i \le N_z) = 0$ and $D_j(-, i > N_z) = \delta_{i-N_z,j}$. Then, from Eq. (50), we get $\tilde{\Phi}_u(\pm) = \mathcal{L}^{-1}D_u(\pm)$.

With the above definitions, the self-energies can then be obtained as,[35]

$$\Sigma_L = V\mathcal{K}^{-1}(-), \quad \Sigma_R = V^\dagger\mathcal{K}^1(+). \tag{52}$$

We remark that the $G^{r/a}$ in Eq. (47) can be simplified by using these self-energies[34]. Additionally, the block Green's function for the left semi-infinite ZGR can be written as

$$\begin{aligned} G_{m,0}^L(\varepsilon) &\equiv \langle m|\frac{1}{\varepsilon + i0_+ - H_L}|0\rangle \\ &= \mathcal{K}^m(-)g(\varepsilon + i0_+), \quad m < 0, \end{aligned} \tag{53}$$

with $g(\varepsilon + i0_+)$ being the surface Green's function given by

$$g(\varepsilon + i0_+) = \mathcal{K}^{-1}(-)(V^\dagger)^{-1}. \tag{54}$$

Analogously, for the right semi-infinite ZGR, we have

$$G_{m,1}^R(\varepsilon) \equiv \langle m|\frac{1}{\varepsilon + i0_+ - H_R}|1\rangle = \mathcal{K}^m(+)V^{-1}, \quad m \ge 1. \tag{55}$$

Moreover, the retarded Green's function for an infinite ideal ZGR, $G^0_{m,m'}(\varepsilon)$, can also be easily obtained using the bulk modes. We have[35]

$$G^0_{m,m'}(\varepsilon) = \{\theta(m-m')\mathcal{K}^{m-m'}(+) + \theta(m'-m)\mathcal{K}^{m-m'}(-)\} \cdot \left\{V^\dagger[\mathcal{K}(-)-\mathcal{K}(+)]\right\}^{-1}, \quad (56)$$

where $\theta(x)$ denotes the Heaviside step function.

V. SUMMARY

We have obtained complete sets of BMs for graphene and graphene ribbons (both ZGR and AGR) at arbitrary energy ε. These modes are presented in a representation that is particularly suitable for studying the electronic conduction of graphene nanostructures. Their properties have been thoroughly analyzed and analytical expressions for low-energy ZGR BMs have been prescribed. At fixed energy, each BM can be specified by a single parameter σ (while the λ is determined from σ and therefore not a free parameter), which (in ZGR) is shown to satisfy a simple polynomial equation that can be efficiently solved with existing numerical techniques.

The utility of the BMs is illustrated in a few examples, by which we demonstrated that they could be used to construct the electronic band structure of graphene nanostructures, to calculate the transmission matrix of graphene devices and to evaluate the Green's functions of both infinite and semi-infinite graphene ribbons. These Green's functions play an important role in modern mesoscopic transport theory. We also note that the BMs can be used to construct the transfer matrix in the so-called transfer-matrix method,[55–57] which is basically a variation of the mode-matching method.

Moreover, exploring the feature of the wave functions for BMs may offer intuitive understanding of some otherwise perplexing phenomena, as demonstrated in the case of transmission through bends and polygons[37] and current blocking effect in ZGR p-n junctions.[48]

Acknowledgments

K. W. acknowledges the financial support by Grant-in-Aid for Scientific Research from MEXT and JSPS (Nos. 25107001, 25107005 and 23310083).

Appendix A: Bulk Modes and Green's functions of Armchair Graphene Ribbons

1. Bulk Modes

We consider an AGR extended in the y-direction but confined between $m = 0$ and $m = N_a + 1$, as depicted in Fig. 6. We may include only the left half of the $(N_a + 1)$-th supercell. In close analogy with Eq.(17), we write the bulk modes as

$$\hat{\varphi}(m,n;\lambda,\sigma,s) \coloneqq \sigma^n\left(\beta\lambda^m\hat{M} - \beta'\lambda^{-m}\hat{M}^{-1}\right)\hat{f}_{\lambda\sigma s}, \quad (A1)$$

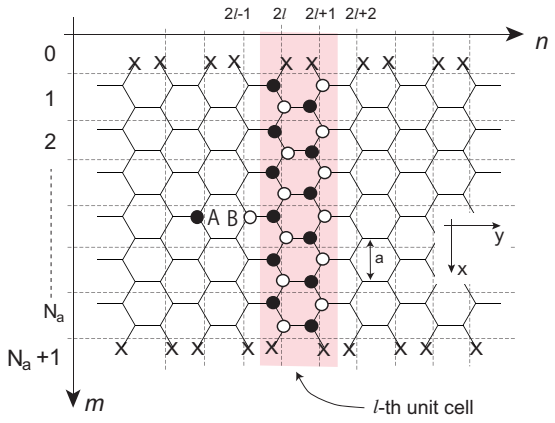

FIG. 6: Lattice structure of armchair graphene ribbons.

where β and β' are coefficients to be determined using the boundary condition. Here we have used that $\hat{f}_{\lambda\sigma s} = \hat{f}_{\lambda^{-1}\sigma s}$ as well as $M(\lambda^{-1}) = M^{-1}(\lambda)$. $\hat{\varphi}(m,n;\lambda,\sigma,s)$ is a spinor, which is defined as

$$\hat{\varphi}(m,n;\lambda,\sigma,s) = \begin{pmatrix} \varphi_{\rm A}(m,n;\lambda,\sigma,s) \\ \varphi_{\rm B}(m,n;\lambda,\sigma,s) \end{pmatrix}. \quad (A2)$$

In the following, we simply write $\hat{\varphi}(m,n)$ and $\varphi_\nu(m,n)$ (ν = A, B) instead of $\hat{\varphi}(m,n;\lambda,\sigma,s)$ and $\varphi_\nu(m,n;\lambda,\sigma,s)$, respectively, if there is no ambiguity. The B.C. for AGR is written as

$$\begin{aligned} &\varphi_{\rm A}(0,2l-1) = 0, \qquad &&\varphi_{\rm B}(0,2l) = 0, \\ &\varphi_{\rm A}(N_a+1,2l-1) = 0, \quad &&\varphi_{\rm B}(N_a+1,2l) = 0, \end{aligned} \quad (A3)$$

where l is any integer (see Fig. 6). Note that if the left half of the $(N_a + 1)$-th supercell is excluded, the latter two conditions have to be changed to

$$\varphi_{\rm B}(N_a+1,2l-1) = 0, \quad \varphi_{\rm A}(N_a+1,2l) = 0. \quad (A4)$$

Nevertheless, basically the same results occur and hence we here ignore this case. From these conditions, we find

$$\begin{aligned} \beta\lambda^{1/4} - \beta'\lambda^{-1/4} &= 0, \\ \beta\lambda^{1/4}\lambda^{N_a+1} - \beta'\lambda^{-1/4}\lambda^{-(N_a+1)} &= 0. \end{aligned} \quad (A5)$$

It immediately follows that

$$\lambda^{2(N_a+1)} = 1, \quad (A6)$$

which demands λ to be a simple phase factor. Thus, we may put $\lambda = \lambda_j = e^{ik_j}$, with $k_j = \frac{\pi}{N_a+1}\cdot j$, where $j = 1, ..., N_a + 1$, leading to $(N_a + 1)$ pairs of subbands. From this, the $\sigma = \sigma_j$ is then determined by Eq.(13), which yields

$$\sigma_j \coloneqq \frac{1}{2}\left\{\zeta_j^2 - 2 \pm \sqrt{\zeta_j^2(\zeta_j^2-4)}\right\}, \quad (A7)$$

where $\zeta_j = \frac{\varepsilon^2 - 1 - g_{k_j}^2}{g_{k_j}}$ with $g_k = 2\cos(k/2)$. We shall use $\sigma_j(+)$ [$\sigma_j(-) = \sigma_j^{-1}(+)$] to denote the left- (right-) going modes.

Now we obtain

$$\hat{\varphi}_{js}(m,n) \coloneqq \hat{\varphi}(m,n;\lambda_j,\sigma_j,s) = \sigma_j^n \times \begin{pmatrix} \sin[k_j(m-\frac{(-1)^n+1}{4})] & 0 \\ 0 & \sin[k_j(m+\frac{(-1)^n-1}{4})] \end{pmatrix} \hat{f}_{\lambda_j\sigma_j s} \tag{A8}$$

where an irrelevant factor has been absorbed in the normalization factor of $f_{\lambda_j\sigma_j s}$.

2. Green's functions

We proceed to establish the Green's functions of AGR by the BMs. To this end, we need to adapt Eq.(A8) into a form that fits the AGR unit cell as defined by the underlying translational symmetry. An AGR unit cell, indexed by l, consists of two adjacent zigzag chains, $n = 2l$ and $n = 2l+1$, instead of one. Let us consider the unit cell $l = 0$, which contains the 0-th and 1-st zigzag chains. We may arrange the values of $\hat{\varphi}_{js}(m,0)$ into a $2(N_a+1)$ column vector Φ_j^0, defined as

$$\Phi_j^0 := [\varphi_A(1,0;j),\varphi_B(1,0;j),...,\varphi_A(N_a,0;j),\varphi_B(N_a,0;j), \varphi_A(N_a+1,0;j),0]^T, \tag{A9}$$

where $\varphi_\nu(m,n;j) \coloneqq \varphi_\nu(m,n;\lambda_j,\sigma_j,s)$. Similarly, we define

$$\Phi_j^1 := [\varphi_A(1,1;j),\varphi_B(1,1;j),...,\varphi_A(N_a,1;j),\varphi_B(N_a,1;j), \varphi_A(N_a+1,1;j),0]^T. \tag{A10}$$

Now we merge Φ_j^0 and Φ_j^1 in a single $4(N_a+1)\times 1$ column vector,

$$\Phi_j := \begin{pmatrix} \Phi_j^0 \\ \Phi_j^1 \end{pmatrix}, \tag{A11}$$

which is no more than the wave function of the j-th mode for the unit cell $l = 0$. For an arbitrary unit cell, the wave function can also be written as a $4(N_a+1)\times 1$ column vector, $\varphi_j(l)$, which isrelated to $\varphi_j(l=0) = \Phi_j$ as follows,

$$\varphi_j(l) = \tilde{\sigma}_j^l \Phi_j, \tag{A12}$$

where $\tilde{\sigma}_j = \sigma_j^2$. Following scrupulously Ref.[34], we hereafter write $\Phi_j(\pm)$ in regard to $\tilde{\sigma}_j(\pm) = \sigma_j^2(\pm)$. Now we define the vectors $\tilde{\Phi}_j(\pm)$ which are dual to $\Phi_j(\pm)$,

$$\tilde{\Phi}_j^\dagger(\pm)\Phi_{j'}(\pm) = \delta_{j,j'}, \quad \Phi_j^\dagger(\pm)\tilde{\Phi}_{j'}(\pm) = \delta_{j,j'}. \tag{A13}$$

These $\tilde{\Phi}_j(\pm)$ can be written as a merger of two $2(N_a+1)\times 1$ vectors, $[\tilde{\Phi}_j^>(\pm),\tilde{\Phi}_j^<(\pm)]^T$, where $\tilde{\Phi}_j^<$ can be determined from $\tilde{\Phi}_j^>$, due to the fact that $\Phi_j(i)$ and $\Phi_j(i+2(N_a+1))$ are related, as is clear from Eq. (A8). Finally, the vectors $\Phi_j(\pm)$ and $\tilde{\Phi}_j(\pm)$ are used to construct the $\mathcal{K}$ matrice,

$$\mathcal{K}^r(\pm) = \sum_{j=1}^{2(N_a+1)} \tilde{\sigma}_j^r(\pm)\Phi_j(\pm)\tilde{\Phi}_j^\dagger(\pm), \tag{A14}$$

with r being an integer. Finally, with Eq. (A14), the Green's functions for infinite and semi-infinite AGRs can be written down in exactly the same form as Eqs. (52)-(56), except that one replaces m by l and V by the coupling between adjacent AGR unit cells.

Appendix B: Alternative Expressions for Group Velocity

It is essential to calculate the group velocity of each mode in evaluating the transmission matrix. Although this velocity can be computed using Eq. (32), we feel it more convenient to adopt an alternative expression in numerical simulations. Below we derive this expression. We shall first lay down the formulation for general lattices and then specify it to ZGRs.

Consider a general Bravais lattice, each site of which is labelled by the corresponding position vector $\vec{R}$. Let the Hamiltonian be

$$\hat{H} = \sum_{\vec{R},\vec{R}'} H(\vec{R},\vec{R}')|\vec{R}\rangle\langle\vec{R}'|. \tag{B1}$$

We write the position operator of an electron as

$$\hat{x} = \sum_{\vec{R}} \vec{R}|\vec{R}\rangle\langle\vec{R}|. \tag{B2}$$

The velocity operator is then defined to be

$$\hat{V} = \dot{\hat{x}} = -i[\vec{x},\hat{H}] =: \vec{v}(\vec{R},\vec{R}')|\vec{R}\rangle\langle\vec{R}'|, \tag{B3}$$

with

$$\vec{v}(\vec{R},\vec{R}') = -i\sum_{\vec{R},\vec{R}'}(\vec{R}-\vec{R}')H(\vec{R},\vec{R}'). \tag{B4}$$

Now the group velocity of any state $|\psi\rangle$ is given by

$$\vec{v}_g = \langle\psi|\hat{V}|\psi\rangle = -i\sum_{\vec{R},\vec{R}'}\psi^*(\vec{R})(\vec{R}-\vec{R}')H(\vec{R},\vec{R}')\psi(\vec{R}'), \tag{B5}$$

where $\psi(\vec{R})$ denotes the wave function of the state.

Now we apply Eq. (B5) to ZGRs. We replace $\psi(\vec{R})$ by Eq. (31) and after some algebra, we obtain the group velocity (in the x-direction) assigned to the mode $\hat{\psi}(m,n;k,p,s)$ as follows,

$$v_{ps}(k) \propto -s(-1)^Q \sin\left(\frac{k}{2}\right)\sum_n \sin\left(p\,(N_z+1-n)\right)\sin\left(pn\right), \tag{B6}$$

up to an irrelevant constant. This expression does not involve a derivative and is hence more convenient in numerical computations. The group velocity vanishes in the y-direction expectedly.

* Corresponding author: WAKABAYASHI.Katsunori@nims.go.jp

1 K. S. Novoselov, A. K. Geim, S. V. Morozov, D. Jiang, Y. Zhang, S. V. Dubonos, I. V. Grigorieva, and A. A. Firsov, Science **306**, 666 (2004).

2 K. Novoselov, D. Jiang, F. Schedin, T. Booth, V. Khotkevich, S. Morozov, and A. Geim, Proc. Natl. Acad. Sci. USA **102**, 10451 (2005).

3 K. Novoselov, A. K. Geim, S. Morozov, D. Jiang, M. Katsnelson, I. Grigorieva, S. Dubonos, and A. Firsov, Nature **438**, 197 (2005).

4 M. Fujita, K. Wakabayashi, K. Nakada, and K. Kusakabe, J. Phys. Soc. Jpn. **65**, 1920 (1996).

5 K. Nakada, M. Fujita, G. Dresselhaus, and M. S. Dresselhaus, Phys. Rev. B **54**, 17954 (1996).

6 K. Wakabayashi, M. Fujita, H. Ajiki, and M. Sigrist, Phys. Rev. B **59**, 8271 (1999).

7 K. Wakabayashi, M. Sigrist, and M. Fujita, J. Phys. Soc. Jpn. **67**, 2089 (1998).

8 C. L. Kane and E. J. Mele, Phys. Rev. Lett. **95**, 146802 (2005).

9 K. Wakabayashi, Y. Takane, and M. Sigrist, Phys. Rev. Lett. **99**, 036601 (2007).

10 D. A. Areshkin, D. Gunlycke, and C. T. White, Nano Letters **7**, 204 (2007).

11 K. Wakabayashi, Y. Takane, M. Yamamoto, and M. Sigrist, Carbon **47**, 124 (2009).

12 K. Wakabayashi, Y. Takane, M. Yamamoto, and M. Sigrist, New J. Phys. **11**, 095016 (2009).

13 A. K. Geim and K. S. Novoselov, Nat. Mater. **6**, 183 (2007).

14 A. C. Neto, F. Guinea, N. Peres, K. S. Novoselov, and A. K. Geim, Rev. Mod. Phys. **81**, 109 (2009).

15 K. Wakabayashi and S. Dutta, Solid State Comm. **152**, 1420 (2012).

16 H. Raza, ed., *Graphene Nanoelectronics*, Vol. 1 (Springer, 2012).

17 V. V. Cheianov and V. I. Fal'ko, Phys. Rev. B **74**, 041403 (2006).

18 D. A. Abanin and L. S. Levitov, Science **317**, 641 (2007).

19 H.-Y. Deng, J. Appl. Phys. **111**, 033706 (2012).

20 D. Gunlycke, D. A. Areshkin, J. Li, J. W. Mintmire, and C. T. White, Nano Letters **7**, 3608 (2007).

21 D. A. Areshkin and C. T. White, Nano Letters **7**, 3253 (2007).

22 B. Özyilmaz, P. Jarillo-Herrero, D. Efetov, D. A. Abanin, L. S. Levitov, and P. Kim, Phys. Rev. Lett. **99**, 166804 (2007).

23 B. Huard, J. A. Sulpizio, N. Stander, K. Todd, B. Yang, and D. Goldhaber-Gordon, Phys. Rev. Lett. **98**, 236803 (2007).

24 J. R. Williams, L. DiCarlo, and C. M. Marcus, Science **317**, 638 (2007).

25 J. T. Londergan, J. P. Carini, and D. P. Murdock, *Binding and scattering in two-dimensional systems: applications to quantum wires, waveguides and photonic crystals*, Vol. 60 (Springer, 1999).

26 R. Landauer, IBM J. Res. Deve. **1**, 223 (1957).

27 R. Landauer, Philos. Mag. **21**, 863 (1970).

28 M. Büttiker, Phys. Rev. Lett. **57**, 1761 (1986).

29 T. Ando, Phys. Rev. B **44**, 8017 (1991).

30 M. Zwierzycki, P. A. Khomyakov, A. A. Starikov, K. Xia, M. Talanana, P. X. Xu, V. M. Karpan, I. Marushchenko, I. Turek, G. E. W. Bauer, G. Brocks, and P. J. Kelly, physica status solidi (b) **245**, 623 (2008).

31 H. H. B. Sørensen, P. C. Hansen, D. E. Petersen, S. Skelboe, and K. Stokbro, Phys. Rev. B **79**, 205322 (2009).

32 E. N. Economou and C. M. Soukoulis, Phys. Rev. Lett. **46**, 618 (1981).

33 D. S. Fisher and P. A. Lee, Phys. Rev. B **23**, 6851 (1981).

34 S. Datta, *Electronic transport in mesoscopic systems* (Cambridge university press, 1997).

35 P. Khomyakov, G. Brocks, V. Karpan, M. Zwierzycki, and P. Kelly, Phys. Rev. B **72**, 035450 (2005).

36 J. Wurm, M. Wimmer, İ. Adagideli, K. Richter, and H. U. Baranger, New J. Phys. **11**, 095022 (2009).

37 A. Iyengar, T. Luo, H. A. Fertig, and L. Brey, Phys. Rev. B **78**, 235411 (2008).

38 L. Brey and H. A. Fertig, Phys. Rev. B **73**, 235411 (2006).

39 C. W. J. Beenakker, Rev. Mod. Phys. **69**, 731 (1997).

40 M. Yamamoto and K. Wakabayashi, Appl. Phys. Lett. **95**, 082109 (2009).

41 A. Rycerz, J. Tworzydło, and C. Beenakker, Nat. Phys. **3**, 172 (2007).

42 K. Wakabayashi and M. Sigrist, Phys. Rev. Lett. **84**, 3390 (2000).

43 In numerical scheme, Eq. (23) can lead to ambiguity in calculating the parity. Take propagating modes for example, i.e., $\lambda = e^{ik}$. The parity does not depend on k and can be evaluated at e.g. $k = \pi$, where $\Lambda = 0$ and $p = \frac{\pi}{N_z} \cdot r$, with $r = 1, ..., N_z$ being an integer. Hence, $(-1)^Q = (-1)^r \cdot \sigma^{-1} \sqrt{\sigma^2} = (-1)^r \cdot \sigma^{-1} \cdot (\pm\sigma) = \pm \cdot (-1)^r$, where the amiguity about the sign can be removed by fixing it to be plus. The computer, however, may be ill in doing this and can produce messy results. Therefore, it is crucial to ensure that $\sqrt{\sigma^2} = \sigma$ in programming.

44 The ε_{max} occurs at $k = 0$, i.e., $\Lambda = 2$. Then, by Eq. (13), $\varepsilon_{max}^2 = 5 + 4\cos(\phi)$. The ϕ plays the role in $\cos(\phi) = -\frac{1}{2} - \frac{\sin(\phi)}{\tan(N_z\phi)}$, as inferred from Eq. (25). Assume $\phi = \frac{\pi}{N_z} - \delta$, where $0 < \delta \ll \frac{\pi}{N_z}$, and we have $\cos(\frac{\pi}{N_z} - \delta) = \frac{\sin(\frac{\pi}{N_z} - \delta)}{\tan(N_z\delta)} - \frac{1}{2}$. For very large N_z, this translates into $\delta \approx \frac{2\pi}{N_z(3N_z+2)}$, which is indeed much smaller than $\frac{\pi}{N_z}$ as presumed. Upon subtitution, we arrive at the ε_{max} given in the main text.

45 To prove this, one may show that the companion matrix of the polynomial is irreducible. Note that this polynomial can be written as $P(x) = \sum_{j=0}^{2N_z} C_j x^j$, where $C_j = 1 + j$ for $j < N_z$, $C_j = N_z + 1 - \frac{1}{\varepsilon^2}$ for $j = N_z$ and $C_j = 2N_z + 1 - j$ for $j > N_z$.

46 A. Akhmerov, J. Bardarson, A. Rycerz, and C. Beenakker, Phys. Rev. B **77**, 205416 (2008).

47 K. Wakabayashi and T. Aoki, Int. J. Mod. Phys. B **16**, 4897 (2002).

48 H.-Y. Deng, K. Wakabayashi, and C.-H. Lam, J. Phys. Soc. Jpn. **82**, 104707 (2013).

49 I. O. Kerner, Numer. Math. **8**, 290 (1966).

50 É. Durand, Paris: Masson, 1972 **1** (1972).

51 D. Klein, Chem. Phys. Lett. **217**, 261 (1994).

52 K. Wakabayashi, Phys. Rev. B **64**, 125428 (2001).

53 H.-Y. Deng, K. Wakabayashi, and C.-H. Lam, Phys. Rev. B **89**, 045423 (2014).

54 C. Caroli, R. Combescot, P. Nozieres, and D. Saint-James, J. Phys. C: Solid State **4**, 916 (1971).

55 G. J. Ferreira, M. N. Leuenberger, D. Loss, and J. C. Egues, Phys. Rev. B **84**, 125453 (2011).

56 A. R. Hernández and C. H. Lewenkopf, Phys. Rev. B **86**, 155439 (2012).

57 S. Grover, S. Ghosh, and M. Sharma, Modelling Simul. Mater. Sci. Eng. **20**, 045010 (2010).